ACS APPLIED MATERIALS & INTERFACES

Research Article

Cite This: ACS Appl. Mater. Interfaces 2018, 10, 43970−43977

www.acsami.org

Hybrid Magnetodynamical Modes in a Single Magnetostrictive Nanomagnet on a Piezoelectric Substrate Arising from Magnetoelastic Modulation of Precessional Dynamics

Sucheta Mondal,[†] Md Ahsanul Abeed,[‡] Koustuv Dutta,[†] Anulekha De,[†] Sourav Sahoo,[†] Anjan Barman,*[,†] and Supriyo Bandyopadhyay*[,‡]

[†]Department of Condensed Matter Physics and Material Sciences, S. N. Bose National Centre for Basic Sciences, Block JD, Sector III, Salt Lake, Kolkata 700106, India

[‡]Department of Electrical and Computer Engineering, Virginia Commonwealth University, Richmond, Virginia 23284, United States

Supporting Information

ABSTRACT: Magnetoelastic (or "straintronic") switching has emerged as an extremely energy-efficient mechanism for switching the magnetization of magnetostrictive nanomagnets in magnetic memory and logic, and non-Boolean circuits. Here, we investigate the ultrafast magnetodynamics associated with straintronic switching in a single quasielliptical magnetostrictive Co nanomagnet deposited on a piezoelectric $Pb(Mg_{1/3}Nb_{2/3})$-O_3−$PbTiO_3$ substrate using time-resolved magneto-optical Kerr effect (TR-MOKE) measurements. The pulsed laser pump beam in the TR-MOKE plays a dual role: it causes precession of the nanomagnet's magnetization about an applied bias magnetic field and it also generates surface acoustic waves in the piezoelectric substrate that produce periodic strains in the magnetostrictive nanomagnet and modulate the precessional dynamics. This modulation gives rise to intriguing hybrid magnetodynamical modes in the nanomagnet, with a rich spin-wave texture. The characteristic frequencies of these modes are 5−15 GHz, indicating that strain can affect magnetization in a magnetostrictive nanomagnet in time scales much smaller than 1 ns (~100 ps). This can enable ~10 GHz range magnetoelastic nano-oscillators that are actuated by strain instead of a spin-polarized current, as well as ultrafast magnetoelectric generation of spin waves for magnonic logic circuits, holograms, etc.

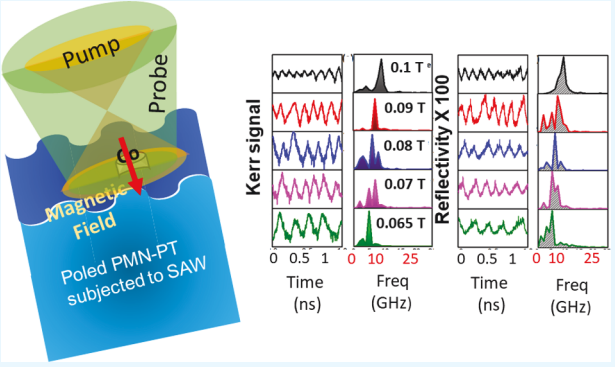

KEYWORDS: *precessional magnetodynamics, magnetoelastic coupling, straintronics, magnetic nanostructures, time-resolved magneto-optical Kerr effect, spin-wave modes*

1. INTRODUCTION

Nanomagnetic switches are potential replacements for the celebrated transistor in computing and signal processing hardware because they are energy-efficient switches that are also nonvolatile. Nanomagnets exhibit interesting spin configurations, such as quasisingle domain configurations, vortices, skyrmions, and magnetic monopole defects.[1−3] A wide variety of dynamics can occur in them over a broad time scale, e.g., ultrafast demagnetization, remagnetization, precession, damping, and domain wall movement,[4] all of which have their own intriguing applications[5,6]

A nanomagnet's magnetization can be switched with an external agent in a variety of ways, among which an extremely energy-efficient approach is "straintronics".[7−9] Here, the magnetization of a magnetostrictive nanomagnet is switched with mechanical strain (Villari effect) via elastic coupling to an underlying piezoelectric substrate that is activated by a voltage.[7−11] Although this methodology has attracted attention because of its excellent energy efficiency, to our knowledge, there has been no experimental study of the ultrafast magnetization dynamics associated with straintronic switching, even though nonstraintronic magnetization reversal and dynamics of large arrays of nanomagnets[12] or even single nanomagnets have been extensively studied.[13−15] Here, we report the study of ultrafast strain-modulated magnetization dynamics in a single magnetostrictive Co nanomagnet fabricated on a (001) $Pb(Mg_{1/3}Nb_{2/3})O_3$−$PbTiO_3$ (PMN−PT) piezoelectric substrate, performed using time-resolved magneto-optical Kerr effect (TR-MOKE) measurements. These studies elucidate the temporal dynamics of strain-induced magnetization rotation and reveal the time scales associated with switching. In our study, we chose Co as the magnetostrictive nanomagnet, despite its relatively weak magnetostriction, since it is a single element and not an

Received: November 2, 2018
Accepted: November 23, 2018
Published: November 23, 2018

DOI: 10.1021/acsami.8b19243
ACS Appl. Mater. Interfaces 2018, 10, 43970−43977

alloy. Alloys such as GaFe and Terfenol-D have much higher magnetostriction than Co, but they have multiple phases (not all of which produce high magnetostriction) and also pinning sites that pin the magnetization and inhibit magnetization dynamics.[16] For these reasons, Co is better suited to this study.

In our TR-MOKE setup, a femtosecond laser pump beam excites the magnetization of the Co nanomagnet to precess about an applied bias magnetic field. At the same time, the alternating electric field in that same beam also generates periodic (compressive and tensile) strain in the PMN−PT substrate from d_{33} and/or d_{31} coupling. This happens because the laser electric field periodically reconfigures the charge distribution on the surface of the PMN−PT substrate and that, in turn, modulates the electric field within the substrate via the Poisson equation. Since PMN−PT is piezoelectric and has been poled, the periodically modulated electric field within the substrate will produce a periodic strain due to d_{33} and d_{31} coupling. The strain will alternate between tensile and compressive (strain is tensile if the electric field in the substrate is in the same direction as poling and compressive if the electric field is opposite to the direction of poling). Additional periodic strain is generated in the substrate (underneath the nanomagnet) from the differential thermal expansions of the nanomagnet and the substrate due to periodic heating by the pulsed pump beam.[16−18] This thermally generated strain is, however, always tensile in the substrate in our experiment (its magnitude varies periodically, but the sign does not change) because the thermal coefficient of expansion of Co (13×10^{-6}/K) is greater than that of PMN−PT (9.5×10^{-6}/K). Note that the former mechanism requires a piezoelectric substrate whereas the latter does not. Another distinction is that in the former case, the strains in the substrate and nanomagnet have the same sign whereas in the latter case, they have opposite signs. The latter mechanism has been studied in some earlier work,[17−20] but the former has not. In our system, the former is expected to be dominant (see the Supporting Information) and hence, to our knowledge, this is the first study of this effect.

The total periodic strain produced in the substrate owing to both mechanisms generates surface acoustic waves (SAWs)[17−20] that periodically expand and contract the nanomagnet sitting on the substrate and change its magnetization owing to the Villari effect.[21,22] In the end, two distinct sources induce oscillations in the out-of-plane component of the nanomagnet's magnetization: the Villari effect associated with the SAW and the magnetization precession about the bias magnetic field that can be set off by the laser-induced optical pumping. The interaction of these two oscillations gives rise to multiple hybrid magnetodynamical oscillation modes (each with its own characteristic frequency) in the out-of-plane component of the magnetization, which then induce corresponding oscillations in the nanomagnet's reflectivity and polarization of the reflected light (Kerr signal). The periods of these oscillations are found to be 70−200 ps, which suggest that the magnetization of the nanomagnet can respond to SAW-induced strain in time scales on the order of 100 ps. This is an important insight since SAW-based magnetization switching has attracted significant interest owing to its many applications.[23−38]

Our study also revealed that the spin waves that are excited in the nanomagnet in the form of hybrid magnetodynamical modes exhibit complex power and phase profiles owing to the mixing of the precessional magnetodynamics and SAW-induced magnetodynamics.

To investigate the hybrid modes experimentally, we fabricated an array of slightly elliptical (eccentricity ≈1) Co nanomagnets (magnetostriction χ = 40−60 ppm) on a piezoelectric (001) PMN−PT substrate (d_{33} > 2000 pC/N). The thickness of the nanomagnets is nominally 15 nm. Figure 1a,b shows a scanning electron micrograph of the nanomagnets and their magnetic force microscope (MFM) images. The nanomagnets are almost circular with a major axis of 190 nm and minor axis of 186 nm. Because of this small aspect ratio, they do not show a good phase contrast in the MFM images or single domain behavior, but because their shape anisotropy is small, the magnetic anisotropy is dominated by strain anisotropy in the presence of the SAWs. The spacing between neighboring nanomagnets (∼1 μm) is large enough for the dipole interaction between them to be negligible, which means that magnetically isolated single nanomagnets are probed.

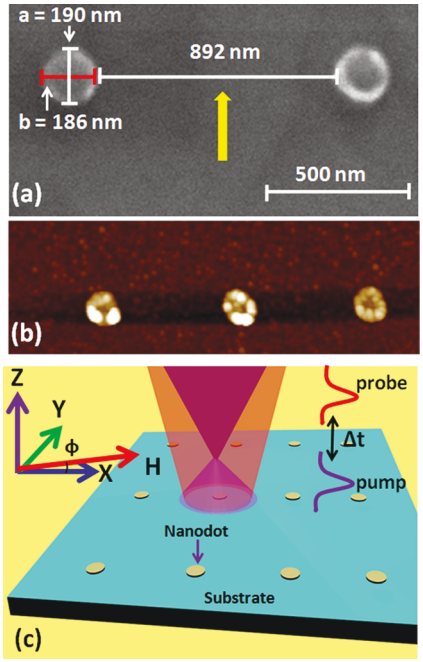

Figure 1. (a) Scanning electron micrograph of the Co nanomagnets deposited on a PMN−PT substrate. The edge-to-edge separation between two neighboring nanomagnets in a row (along the line collinear to their minor axis (x direction)) is about 892 nm, which shows that the pitch of the array is about 1 μm. The separation between two adjacent rows is ∼4 μm along the y direction. Major and minor axes are denoted as a (≈190 nm) and b (≈186 nm), respectively. The yellow arrow indicates the poling direction of the substrate. (b) Magnetic force micrograph of the nanomagnets that does not show a good phase contrast because of insufficient shape anisotropy. (c) The experimental geometry is shown with the bias magnetic field (H) applied along the array in the direction of the nanomagnets' minor axes (x direction) with a slight out-of-plane tilt (ϕ) of a few degrees.

2. EXPERIMENTAL SECTION

To ascertain that the pump beam indeed generates SAWs in the PMN−PT substrate, we first measured the polarization and intensity of light reflected from the bare PMN−PT substrate as a function of the delay between the pump and the probe by focusing both pump and probe beams on to the bare substrate. Clear oscillations are

DOI: 10.1021/acsami.8b19243
ACS Appl. Mater. Interfaces 2018, 10, 43970−43977

observed in both polarization and intensity of the light reflected from the bare substrate and they can only originate from the SAWs. In Figure 2a, we show the intensity (reflectivity) oscillation for a 15 mJ/

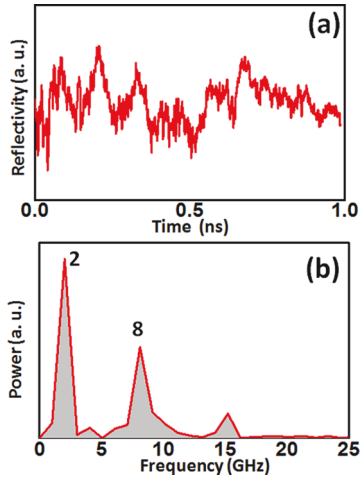

Figure 2. (a) Background-subtracted time-resolved data for reflectivity of the bare PMN−PT substrate as a function of the delay between the pump and the probe, obtained at 15 mJ/cm^2 pump fluence. (b) Also shown are the fast Fourier transforms of the oscillations. Frequencies of the two most intense peaks are indicated in gigahertz.

cm^2 pump fluence (wavelength = 400 nm), whereas the oscillation in the polarization (Kerr signal) is shown in Figure S1 of the Supporting Information. As expected, there are multiple oscillation modes in both reflectivity and polarization, each with a different frequency, because of the excitation of SAWs with multiple frequencies. Their frequencies at any given fluence were found to be independent of the bias magnetic field, showing that these oscillations are not of magnetic origin. They arise from the SAWs that cause periodic atomic displacements on the substrate's surface thereby changing the surface charge polarization periodically (PMN−PT is a polar material), giving rise to polar phonons. The fast Fourier transformation of these oscillations reveals the dominance of two peaks (2 and 8 GHz) in the spectra (see Figure 2b), which we conclude are the two dominant SAW frequencies excited in the PMN−PT substrate by the pulsed pump beam. There is also a small peak in the spectrum at ∼16 GHz, which we ignore (it may be a second harmonic of the 8 GHz oscillation). The SAW wavelength λ associated with the 2 GHz frequency is ascertained from the relation $v = \lambda f$, where v is the phase velocity of the SAW and f is the frequency. The phase velocity of SAW in a (001) PMN−PT crystal depends on the propagation direction, but it is of the order of 2000 m/s.[39] The 2 GHz mode therefore corresponds to a wavelength of roughly 1 μm, which happens to be the pitch of the array. It therefore appears that this mode is a resonant mode determined by the geometry of the array, as in refs17−19. The 8 GHz mode cannot be related to any obvious geometric feature of the nanomagnet array and may be intrinsic to the substrate.

We next probe the out-of-plane magnetization dynamics (temporal variation in the spatially averaged out-of-plane component of the magnetization) of a single Co nanomagnet on the PMN−PT substrate in the presence of both a bias magnetic field and SAWs by focusing the pump and probe beams (probe beam wavelength = 800 nm and fluence = 2 mJ/cm^2) on a single nanomagnet and measuring the Kerr oscillations as well as oscillations in the reflectivity. We were able to obtain signals from a single nanomagnet without cavity enhancement. In Figure 3a,b, we show the background-subtracted time-resolved Kerr oscillations in time as a function of bias magnetic field along with their Fourier transforms. The pump fluence was 15 mJ/cm^2. The reflectivity oscillations and their Fourier transforms are shown in Figure S2 of the Supporting Information.

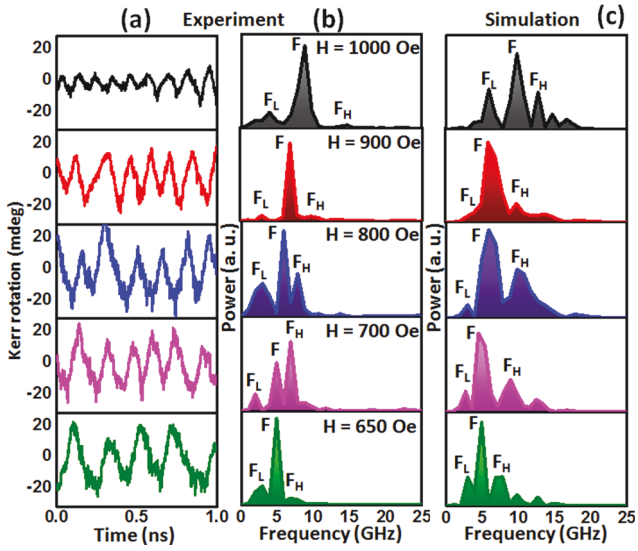

Figure 3. Bias magnetic field dependence of the (background-subtracted) time-resolved Kerr oscillations from a single Co nanomagnet on a PMN−PT substrate. The pump fluence is 15 mJ/cm^2. (a) The measured Kerr oscillations in time and (b) the fast Fourier transforms of the oscillations. The Fourier transform peaks shift to lower frequencies with decreasing bias magnetic field strength. There are multiple oscillation modes of various Fourier amplitudes. Out of those, the dominant mode (at all bias fields except 700 Oe) is denoted by F and its nearest modes F_H and F_L. (c) Fourier transforms of the temporal evolution of the out-of-plane magnetization component at various bias magnetic fields simulated with MuMax3 where the amplitude of the periodically varying strain anisotropy energy density K_0 is assumed to be 22 500 J/m^3. The simulation has additional (weak) higher frequency peaks not observed in the experiment. The spectra in the two right panels are used to compare simulation with experiment.

Multiple modes (corresponding to peaks in the Fourier spectra) are observed in both Kerr and reflectivity oscillations at all bias magnetic fields used, with all peaks shifting to lower frequencies with decreasing bias field. This magnetic field dependence shows that these modes have a magnetic component mixed in. The most intense peak (at all bias fields except 700 Oe) is denoted as "F" in Figure 3b. Two other prominent peaks that appear at higher and lower frequencies with respect to F are indicated as "F_H" and "F_L", respectively. All modes associated with these three peaks in the Fourier spectra are hybrid magnetodynamical modes arising from the interaction between the magnetic (precession of the magnetization about the bias magnetic field) and the nonmagnetic (periodic change in the magnetization due to the periodic strain generated by the SAWs) dynamics. The former dynamics depends on the bias magnetic field, whereas the latter does not. We observed that in all cases, the amplitudes of the reflectivity oscillations are much smaller than those of the Kerr oscillations, as shown in Figure S2 of the Supporting Information.

3. RESULTS AND DISCUSSION

The Kerr and reflectivity oscillations are due to the temporal variation of the spatially averaged out-of-plane component of the magnetization in the nanomagnet. Therefore, to understand the origin of the modes observed in the Kerr and reflectivity oscillations, we have modeled the magnetization dynamics in the Co nanomagnet in the presence of the bias magnetic field and the periodic strain due to the SAWs using the MuMax3 package.[40] The SAW-induced periodic strain anisotropy in the nanomagnet is included in the simulation by making the oscillating strain anisotropy energy density $K_1(t)$ =

DOI: 10.1021/acsami.8b19243
ACS Appl. Mater. Interfaces 2018, 10, 43970−43977

$K_0[\sin(2\pi f_1 t) + \sin(2\pi f_2 t)]$, where $K_0 = (3/2)\chi\sigma$ and f_1, f_2 are the frequencies of the two dominant SAW modes (2 and 8 GHz) observed for the pump fluence of 15 mJ/cm^2. The variation of $K_1(t)$ with time t is shown in Figure S3 of the Supporting Information. Note that the Kerr and reflectivity signals were obtained at the same fluence, which is why we consider the dominant SAW modes at that fluence. We include only two frequency components in the periodic strain anisotropy (f_1 = 2 GHz and f_2 = 8 GHz) since these two frequency components are dominant and have much higher amplitude than that of other components in the SAW signal (as shown in Figure 2). Here, χ is the magnetostriction coefficient of the nanomagnet (40 ppm) and σ is the maximum stress generated in it by the SAW (stress amplitude). There are also some additional contributions to the periodic stress because of the differential thermal expansions of Co and PMN−PT due to periodic heating by the pump beam, which we neglect in this first-order analysis.

We treat K_0 as a fitting parameter. In the MuMax3 modeling, we generate the time-varying components of the nanomagnet's magnetization M_x (x,y,z,t), M_y (x,y,z,t), and M_z (x,y,z,t) for different values of K_0. The minor axis of the nanomagnet is in the x direction, the major axis is along the y direction, and the z direction is the out-of-plane direction. We first generate the micromagnetic distribution within the nanomagnet in the presence of the bias magnetic field applied along the x direction (but with no strain present) from MuMax3. Then, with this distribution as the initial state, we turn on the two-frequency oscillating strain and a small out-of-plane (square-wave) tickle pulse of amplitude 30 Oe, rise time 10 ps, and duration 100 ps to set the magnetodynamics in motion. We find M_x (x,y,z,t), M_y (x,y,z,t), and M_z (x,y,z,t) for different bias magnetic fields and different values of K_0. We then perform fast Fourier transform of the spatially averaged value of M_z (x,y,z,t), which we call $\bar{M}_z(t)$, and the spectra obtained from this transform (for different bias magnetic fields) are shown in Figure 3c. They are compared with the spectra of the Kerr oscillations found experimentally and shown in Figure 3b. This comparison leads us to the best fit value of K_0. We find a reasonably good agreement between the three dominant peaks F_L, F, and F_H of the simulated Kerr spectra and the experimentally measured Kerr spectra for a value K_0 = 22 500 J/m^3 at low bias fields, as shown in Figure 4a. The agreement deteriorates slightly at high bias fields, showing that perhaps a single fitting parameter K_0 is not adequate to model the entire range of bias fields used in the experiments.

From the value K_0 = 22 500 J/m^3, we can also find the effective stress σ generated in the nanomagnet. Since $K_0 = (3/2)\chi\sigma$, we find σ = 375 MPa. We can then find the strain amplitude generated in the nanomagnet from Hooke's law: $\sigma = Y\varepsilon$, where Y is Young's modulus of Co (209 GPa)[41] and ε is the strain amplitude generated by the (polychromatic) SAW. This yields ε = 0.18%. Here, we treat the stress and strain as scalars since we are interested not so much in the accurate stress distribution but rather the maximum uniaxial strain that is generated in any direction. There are reports of strain >0.6% generated in PMN−PT[42] so this large value of strain is not unusual. We can then calculate the effective electric field that would be required to produce the strain of 0.18% in PMN−PT. The reported d_{33} values in PMN−PT are of the order of 2800 pC/N.[43] Hence, the effective electric field E in the PMN−PT substrate (calculated from $\varepsilon = d_{33}E$) is ~6.4 × 10^5 V/m.

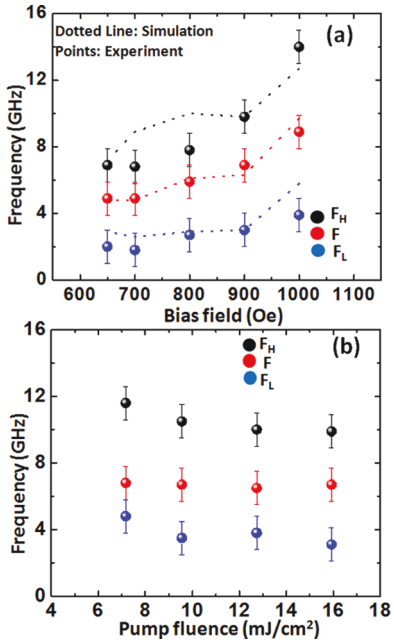

Figure 4. (a) Bias field (H) dependence of the observed three dominant frequencies in the Kerr oscillations F_L, F, and F_H (frequencies of hybrid magnetodynamical modes) at 15 mJ/cm^2 pump fluence. We also show alongside (with a dotted line) the Kerr oscillation frequencies obtained from the MuMax3 modeling based on the assumption K_0 = 22 500 J/m^3. The simulated data points are, for the most part, within the error bars of the experimentally measured data points. (b) Fluence dependence of the frequencies at H = 900 Oe.

In Figure 4b, we show the pump fluence dependencies of the three peak frequencies F_L, F, and F_H in the Kerr oscillation spectra (frequencies of the hybrid magnetodynamical modes) for a bias magnetic field strength of 900 Oe. We expect that the frequency of the magnetic (precessional) component of the mode should depend primarily on the bias magnetic field and hence should be independent of fluence. Since the frequency of the dominant hybrid mode, F (the one with the largest Fourier component at most bias fields) is almost fluence independent and the frequencies of the other two modes are weakly fluence dependent, it appears that the magnetic component of the hybrid mode (the one associated with precessional dynamics) dominates over the nonmagnetic one (the one associated with SAWs) in the hybridization process. This is further supported by the observation that the mode frequencies have a pronounced bias magnetic field dependence, which would not have happened if the nonmagnetic component was dominant. Note, however, that the magnetic field dependence of none of the three dominant mode frequencies (F_L, F, or F_H) could be fitted with the Kittel formula,[44] showing that none is a pure Kittel mode because of the hybridization.

The temporal evolutions of the micromagnetic distributions in the nanomagnet obtained from MuMax3 simulations (see Figure S4 in the Supporting Information) reveal that in the absence of the SAWs, the bias magnetic field will tend to align the magnetization everywhere within the nanomagnet along its own direction, except perhaps at the edges. In the presence of the SAWs, the total field (resultant of bias magnetic field and the periodic effective magnetic field due to strain) periodically changes the orientation of the magnetization, giving rise to spin waves. This will happen even if we ignore the precession

DOI: 10.1021/acsami.8b19243
ACS Appl. Mater. Interfaces 2018, 10, 43970−43977

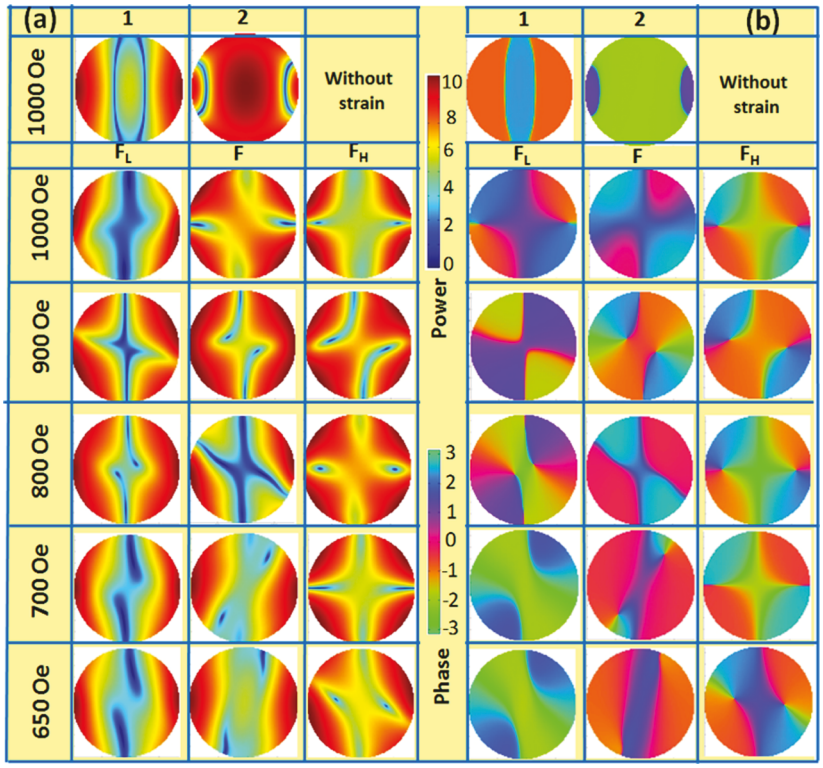

Figure 5. (a) Simulated power and (b) phase profiles of the spin waves associated with the three dominant frequencies F_L, F, and F_H in the Kerr oscillations at any given bias field. The topmost row shows edge and center modes at the two dominant frequencies in the Kerr oscillations in the absence of strain at 1000 Oe bias field. The units of power and phase are decibels and radians, respectively.

around the bias field caused by the femtosecond pump beam excitation. The time-lapsed images in Figure S4 in the Supporting Information correspond to a number of spin-wave modes superposed with appropriate powers and phases.

To gain more insight into the nature of the hybrid magnetodynamical modes associated with the three dominant frequencies in the Kerr oscillations, F_L, F, and F_H, we have calculated the power and phase distributions of the spin waves associated with these modes, using a homebuilt code Dotmag.[45] A description of how Dotmag calculates the power and phase distributions of individual spin-wave modes associated with a given mode frequency is given in the Supporting Information.

We first theoretically examine the unstrained nanomagnet that is not subjected to SAWs and hence experiences pure precessional dynamics because of the bias magnetic field. In this case, the fast Fourier transform of $\bar{M}_z(t)$ reveals two (bias-dependent) dominant frequencies at any given bias magnetic field (see Figure S5a in the Supporting Information). The power and phase distributions of the spin-wave modes associated with these two frequencies are shown in the first row of Figure 5 for a bias magnetic field of 1000 Oe applied along the ellipse's minor axis. These distributions reveal that one of the spin-wave modes in the unstrained nanomagnet is a center mode (mode 2), with power concentrated in the center, and the other is an edge mode (mode 1), with power concentrated at two vertical edges that are perpendicular to the bias field.[46] The bias field dependencies of the frequencies of these two modes can be found in Figure S5b of the Supporting Information and can be fitted with the Kittel formula.[41] The two modes show excellent stability with bias field amplitude.

When the periodic strain anisotropy due to the SAWs (with frequencies of 2 and 8 GHz and energy density amplitude K_0 = 22 500 J/m^3) is introduced, the nature of the spin waves associated with the dominant frequencies F_L, F, and F_H in the Kerr oscillations becomes very different. Instead of center- and edge-mode behavior, the hybrid magnetodynamical modes of frequencies F_L, F, and F_H display complex spin-wave profiles with their unique characteristics. The most intense mode F at 1000 Oe field contains power throughout the nanomagnet, whereas the phase profile suggests that spins precess alternatively in opposite phases, giving rise to the azimuthal contrast with the azimuthal mode quantization number n = 2. On the other hand, the spin waves corresponding to the two modes at frequencies F_L and F_H appear as the modified edge mode and quantized mode of the nanomagnet. As the bias field is reduced, the mode with frequency F starts showing some quantization at the intermediate fields and finally transitions to edge-mode-like behavior in the low-field regime. At an intermediate bias field of H = 800 Oe, the higher frequency mode (F_H) shows an azimuthal character with n = 2. An important feature is that spin-wave power is no longer concentrated along the vertical edges of the nanomagnet like in the conventional edge mode (perpendicular to the applied field) but gets slightly rotated. This is a consequence of having the SAW-induced time-varying strain field present, along with the constant bias field in the system, and their competition. The component of the effective magnetic field due to strain in the ith direction ($i = x, y, z$) is approximately $H^i_{strain}(t) = 3\chi\sigma(t)\, m_i(t)/(\mu_0 M_s) = 2K_1(t)m_i(t)/(\mu_0 M_s)$, where $m_i(t)$ is the ith component of the (spatially averaged) normalized magnetization of the nanomagnet at time t.[47] The amplitude of this field is 409 Oe when K_0 = 22 500 J/m^3. Hence, it is of the same

DOI: 10.1021/acsami.8b19243
ACS Appl. Mater. Interfaces 2018, 10, 43970−43977

order as the bias field when it is at its maximum. The spin-wave profiles in Figure 5 reveal the rich physics of the interaction between the bias field and SAW that produces the hybrid magnetodynamical modes.

4. CONCLUSIONS

In conclusion, we have observed hybrid magnetodynamical modes in a single quasielliptical nanomagnet of Co fabricated on top of a poled (001) PMN−PT substrate due to magnetoelastic modulation of the precessional dynamics. The frequencies of these modes are in the neighborhood of 10 GHz, corresponding to ∼100 ps time scale dynamics. This shows that strain can affect the magnetization state of even a weak magnetostrictive nanomagnet in time scales far shorter than 1 ns. The spin-wave textures of these modes display rich variations with the applied bias field.

Magnetoelectrically generated spin waves have important applications, such as in a magnetoelectric spin-wave amplifier for logic.[48,49] This work sheds light on the practical operating speeds of such devices. This work also has implications for magnetic nano-oscillators that are used as nanoscale microwave generators,[50] spin-wave emitters, and in artificial neural networks.[51] They are usually actuated by a spin-polarized current delivering a spin-transfer torque (STT). One can actuate them with strain, instead of a spin-polarized current, if they are fashioned out of a magnetostrictive nanomagnet elastically coupled to an underlying piezoelectric substrate.[52] Since strain-induced switching is far more energy efficient than spin-transfer torque (STT) switching, such nano-oscillators will dissipate far less energy than their STT counterparts. This work shows that the frequency range of operation of straintronic nano-oscillators can be ∼10 GHz, which makes them an attractive alternative for the more common spin-torque-based nano-oscillators.

Finally, there are other mechanisms at the interface of a ferromagnet and a ferroelectric substrate that can affect the magnetic moments in the ferromagnet. One such mechanism is associated with charge screening at the interface that can affect the magnetic moments or magnetic anisotropy.[53] These mechanisms usually require an epitaxially grown thin ferromagnetic film that has strong bonding at the interface with the ferroelectric substrate. Our structures are not thin films and not epitaxially grown on the PMN−PT substrate. They are amorphous or polycrystalline Co nanostructures deposited (not epitaxially grown) on a ferroelectric substrate by electron-beam evaporation of Co through lithographically delineated windows in a resist. It is therefore very unlikely that these other mechanisms can play any significant role.

Methods. *Sample Preparation.* The nanomagnets were fabricated with electron-beam lithography and electron-beam evaporation of Co, followed by a liftoff. Two different electron-beam resists of different molecular weights were used to facilitate the liftoff. Prior to fabrication, the PMN−PT substrate was poled with a high electric field in the direction of the major axes of the elliptical nanomagnets.

Time-Resolved Magneto-Optical Measurements. A two-color pump−probe technique (pump wavelength = 400 nm, pulse width = 100 fs, repetition rate = 80 MHz; probe wavelength = 800 nm, pulse width = 80 fs, repetition rate = 80 MHz) was used to measure the Kerr rotation and reflectivity signals as a function of time. The spot size of the probe beam was about 800 nm, whereas the pump beam was slightly defocused at the focal plane of the probe beam to obtain a spot size of about 1 μm. It is very important to make the center of the pump beam coincide with that of the probe beam to collect the signal corresponding to uniform excitation. Since the diameter of a nanomagnet is about 190 nm and the pitch of the array is ∼1 μm in a row, the probe beam can be carefully placed and maintained on top of a single nanomagnet using a high-precision $x-y-z$ piezoelectric scanning stage with a feedback loop. We were able to obtain a signal from a single nanomagnet without cavity enhancement. Further measurement details can be found in the Supporting Information.

Micromagnetic Simulations. Micromagnetic simulations are carried out with MuMax3 and Dotmag software. We first run the MuMax3 simulation with the bias magnetic field present but strain absent, for 1 ns to allow the micromagnetic distribution to settle to a steady state. It is verified that running the simulation for a longer time does not change the distribution perceptibly. This distribution is then used as the initial state of the nanomagnet when the oscillating strain and out-of-plane tickle field are turned on in the simulation. The simulation provides the time variation of the (spatially averaged) out-of-plane component of the magnetization $\bar{M}_z(t)$ for any given bias field and oscillating strain anisotropy energy density amplitude K_0. Its Fourier transform spectrum corresponds to that of the Kerr oscillations at that bias field and strain amplitude. The peaks in this spectrum correspond to the (theoretically calculated) frequencies of the hybrid magnetodynamical modes at that bias field and strain amplitude. The points in the dotted lines of Figure 4 are found by this procedure. Note that only the points in the dotted lines at bias fields of 650, 700, 800, 900, and 1000 Oe have been computed and are meaningful. The rest of the points are extrapolations and are a guide to the eye. Further details of the simulators and simulation strategy can be found in the Supporting Information.

■ ASSOCIATED CONTENT

Supporting Information

The Supporting Information is available free of charge on the ACS Publications website at DOI: 10.1021/acsami.8b19243.

Time-resolved magneto-optical measurements, micromagnetic simulations, investigation of SAW generated in the PMN−PT substrate, comparison between the amplitudes of the Kerr signal and reflectivity signals, time-varying strain used in the MuMax3 simulation, time-lapsed micromagnetic distributions obtained from MuMax3 simulations, and simulated spin-wave spectra and mode profiles in an unstrained nanomagnet at various bias magnetic fields (PDF)

■ AUTHOR INFORMATION

Corresponding Authors

*E-mail: abarman@bose.res.in (A.B.).
*E-mail: sbandy@vcu.edu (S.B.).

ORCID

Anjan Barman: 0000-0002-4106-5658
Supriyo Bandyopadhyay: 0000-0001-6074-1212

Author Contributions

S.M., K.D., and A.D. made the time-resolved magneto-optical measurements. M.A.A. fabricated all samples and characterized with magnetic force microscopy. S.M., M.A.A., and S.S. carried out the simulations. A.B. and S.B. supervised the project and formulated the problem. S.M., A.B., and S.B. performed the

DOI: 10.1021/acsami.8b19243
ACS Appl. Mater. Interfaces 2018, 10, 43970−43977

data interpretations. All authors contributed to writing the paper.

Notes

The authors declare no competing financial interest.

■ ACKNOWLEDGMENTS

M.A.A. and S.B. are supported by the U.S. National Science Foundation under grant ECCS-1609303. S.B. also acknowledges the Department of Science and Technology (DST), Government of India, for the VAJRA Faculty Fellowship that enabled his summer visit to the S. N. Bose National Center for Basic Sciences in the summer of 2018. S.M., A.D., and K.D. acknowledge DST, Govt. of India for INSPIRE Fellowship. S.S. acknowledges the S. N. Bose National Center for Basic Sciences for financial support.

■ REFERENCES

(1) Bader, S. D. Opportunities in Nanomagnetism. *Rev. Mod. Phys.* **2006**, *78*, 1−15.
(2) Fert, A.; Cros, V.; Sampaio, J. Skyrmions on the Track. *Nat. Nanotechnol.* **2013**, *8*, 152−156.
(3) Ladak, S.; Read, D. E.; Branford, W. R.; Cohen, L. F.; Branford, W. R. Direct Observation of Magnetic Monopole Defects in an Artificial Spin-ice System. *Nat. Phys.* **2010**, *6*, 359−363.
(4) Barman, A.; Sinha, J. *Spin Dynamics and Damping in Ferromagnetic Thin Films and Nanostructures*; Springer International Publishing, 2018.
(5) Parkin, S. S. P.; Hayashi, M.; Thomas, L. Magnetic Domain-wall Racetrack Memory. *Science* **2008**, *320*, 190−194.
(6) Fernández-Pacheco, A.; Struebel, R.; Fruchart, O.; Hertel, R.; Fischer, P.; Cowburn, R. P. Three-dimensional Nanomagnetism. *Nat. Commun.* **2017**, *8*, No. 15756.
(7) Roy, K.; Bandyopadhyay, S.; Atulasimha, J. Hybrid Spintronics and Straintronics: A Magnetic Technology for Ultralow Energy Computing and Signal Processing. *Appl. Phys. Lett.* **2011**, *99*, No. 063108.
(8) D'Souza, N.; Salehi-Fashami, M.; Bandyopadhyay, S.; Atulasimha, J. Experimental Clocking of Nanomagnets with Strain for Ultralow Power Boolean Logic. *Nano Lett.* **2016**, *16*, 1069−1075.
(9) D'Souza, N.; Biswas, A.; Ahmad, H.; Salehi-Fashami, M.; Al-Rashid, M. M.; Sampath, V.; Bhattacharya, D.; Abeed, M. A.; Atulasimha, J.; Bandyopadhyay, S. Energy-efficient Switching of Nanomagnets for Computing: Straintronics and other Methodologies. *Nanotechnology* **2018**, *29*, No. 442001.
(10) Yang, Y.; Huang, H.; Luo, Z.; Gao, C.; Li, X.; Tao, C. F. Electric Field Control of Magnetic Anisotropy Rotation in Multiferroic Ni/(011)-Pb$(Mg_{2/3}Nb_{1/3})_{0.7}Ti_{0.3}O_3$ Heterostructures. *J. Appl. Phys.* **2017**, *122*, No. 134105.
(11) Yang, S.-W.; Peng, R.-C.; Jiang, T.; Liu, Y.-K.; Feng, L.; Wang, J.-J.; Chen, L.-Q.; Li, X.-G.; Nan, C.-W. Non-volatile 180° Magnetization Reversal by an Electric Field in Multiferroic Heterostructures. *Adv. Mater.* **2014**, *26*, 7091−7095.
(12) Barman, A.; Haldar, A. Time-domain Study of Magnetization Dynamics in Magnetic Thin Films and Micro- and Nanostructures. *Solid State Phys.* **2014**, *65*, 1−108.
(13) Barman, A.; Wang, S.; Maas, J. D.; Hawkins, A. R.; Kwon, S.; Liddle, A.; Bokor, J.; Schmidt, H. Magneto-optical Observation of Picosecond Dynamics of Single Nanomagnets. *Nano Lett.* **2006**, *6*, 2939−2944.
(14) Barman, A.; Wang, S.; et al. Size-dependent Damping in Picosecond Dynamics of Single Nanomagnets. *Appl. Phys. Lett.* **2007**, *90*, No. 202504.
(15) Rana, B.; Kumar, D.; Barman, S.; Pal, S.; Fukuma, Y.; YoshiChika, O.; Barman, A. Detection of Picosecond Magnetization Dynamics of 50 nm Magnetic Dots Down to the Single Dot Regime. *ACS Nano* **2011**, *5*, 9559−9565.
(16) Ahmad, H.; Atulasimha, J.; Bandyopadhyay, S. Electric Field Control of Magnetic States in Isolated and Dipole-coupled FeGa Nanomagnets Delineated on a PMN−PT Substrate. *Nanotechnology* **2015**, *26*, No. 401001.
(17) Yahagi, Y.; Hartenek, B.; Cabrini, S.; Schmidt, H. Controlling Nanomagnet Magnetization Dynamics via Magneto-elastic Coupling. *Phys. Rev. B.* **2014**, *90*, No. 140405(R).
(18) Yahagi, Y.; Berk, C.; Hebler, B.; Dhuey, S.; Cabrinia, S.; Albrecht, M.; Schmidt, H. Optical Measurement of Damping in Nanomagnet Arrays Using Magneto-elastically Driven Resonances. *J. Phys. D: Appl. Phys.* **2017**, *50*, No. 17LT01.
(19) Yahagi, Y.; Hartenek, B.; Cabrini, S.; Schmidt, H. In *Control of Magnetization Dynamics in Patterned Nanostructures with Magneto-elastic Coupling*, Photonic and Phononic Properties of Engineered Nanostructures V; Adibi, A., Lin, S.-Y., Scherer, A., Eds.; Proceedings of SPIE, 2015; Vol. *9371*.
(20) Yang, H. F.; Garcia-Sanchez, F.; Hu, X. K.; Sievers, S.; Bohnert, T.; Costa, J. D.; Tarequzzaman, M.; Ferreira, R.; Bieler, M.; Schumacher, H. W. Excitation and Coherent Control of Magnetization Dynamics in Magnetic Tunnel Junctions Using Acoustic Pulses. *Appl. Phys. Lett.* **2018**, *113*, No. 072403.
(21) Sampath, V.; D'Souza, N.; Bhattacharya, D.; Atkinson, G. M.; Bandyopadhyay, S.; Atulasimha, J. Acoustic Wave Induced Magnetization Switching of Magnetostrictive Nanomagnets from Single-domain to Nonvolatile Vortex States. *Nano Lett.* **2016**, *16*, 5681−5687.
(22) Sampath, V.; D'Souza, N.; Atkinson, G. M.; Bandyopadhyay, S.; Atulasimha, J. Experimental Demonstration of Acoustic Wave Induced Magnetization Switching in Dipole Coupled Magnetostrictive Nanomagnet for Ultralow Power Computing. *Appl. Phys. Lett.* **2016**, *109*, No. 102403.
(23) Roy, K.; Bandyopadhyay, S.; Atulasimha, J. Energy-efficient Mixed Mode Switching of a Multiferroic Nanomagnet, arXiv:1012.0819. arXiv.org e-Print archive. https://arxiv.org/abs/1012.0819 (submitted Dec 03, 2012).
(24) Biswas, A. K.; Bandyopadhyay, S.; Atulasimha, J. Acoustically Assisted Spin Transfer Torque Switching of Nanomagnets: An Energy-efficient Hybrid Writing Scheme for Non-volatile Memory. *Appl. Phys. Lett.* **2013**, *103*, No. 232401.
(25) Davis, S.; Baruth, A.; Adenwalla, S. Magnetization Dynamics Triggered by Surface Acoustic Waves. *Appl. Phys. Lett.* **2010**, *97*, No. 232507.
(26) Li, W.; Buford, B.; Jander, A.; Dhagat, P. Acoustically Assisted Magnetic Recording: A New Paradigm in Magnetic Data Storage. *IEEE Trans. Magn.* **2014**, *50*, No. 2285018.
(27) Li, W.; Buford, B.; Jander, A.; Dhagat, P. Writing Magnetic Patterns with Surface Acoustic Waves. *J. Appl. Phys.* **2014**, *115*, No. 17E307.
(28) Kovalenko, O.; Pezeril, T.; Temnov, V. V. New Concept for Magnetization Switching by Ultrafast Acoustic Pulses. *Phys. Rev. Lett.* **2013**, *110*, No. 266602.
(29) Foerster, M.; Macià, F.; Statuto, N.; Finizio, S.; Hernández-Mínguez, A.; Lendínez, S.; Santos, P. V.; Fontcuberta, J.; Manel Hernàndez, J. M.; Kläui, M.; Aballe, L. Direct Imaging of Delayed Magneto-dynamic Modes Induced by Surface Acoustic Waves. *Nat. Commun.* **2017**, *8*, No. 407.
(30) Bombeck, M.; Salasyuk, A. S.; Glavin, B. A.; Scherbakov, A. V.; Brüggemann, C.; Yakovlev, D. R.; Sapega, V. F.; Liu, X.; Furdyna, J. K.; Akimov, A. V.; Bayer, M. Excitation of Spin Waves in Ferromagnetic (Ga,Mn)As Layers by Picosecond Strain Pulses. *Phys. Rev. B* **2012**, *85*, No. 195324.
(31) Scherbakov, A. V.; Salasyuk, A. S.; Akimov, A. V.; Liu, X.; Bombeck, M.; Brüggemann, C.; Yakovlev, D. R.; Sapega, V. F.; Furdyna, J. K.; Bayer, M. Coherent Magnetization Precession in Ferromagnetic (Ga,Mns)As Induced by Picosecond Acoustic Pulses. *Phys. Rev. Lett.* **2010**, *105*, No. 117204.
(32) Thevenard, L.; Camara, I. S.; Majrab, S.; Bernard, M.; Rovillain, P.; Lemaître, A.; Gourdon, C.; Duquesne, J.-Y. Precessional

DOI: 10.1021/acsami.8b19243
ACS Appl. Mater. Interfaces 2018, 10, 43970−43977

Magetization Switching by a Surface Acoustic Wave. *Phys. Rev. B* **2016**, *93*, No. 134430.
(33) Weiler, M.; Dreher, L.; Heeg, C.; Huebl, H.; Gross, R.; Brandt, M. S.; Goennenwein, S. T. B. Precessional Magnetization Switching by a Surface Acoustic Wave. *Phys. Rev. Lett.* **2011**, *106*, No. 117601.
(34) Janušonis, J.; Chang, C. L.; van Loosdrecht, P. H. M.; Tobey, R. I. Frequency Tunable Surface Magneto Elastic Waves. *Appl. Phys. Lett.* **2015**, *106*, No. 181601.
(35) Singh, U.; Adenwalla, S. Spatial Mapping of Focused Surface Acoustic Waves in the Investigation of High Frequency Strain Induced Changes. *Nanotechnology* **2015**, *26*, No. 255707.
(36) Thevenard, L.; Duquesne, J.-Y; Peronne, E.; von Bardeleben, H. J.; Jaffres, H.; Ruttala, S.; George, J.-M.; Lemaître, A.; Gourdon, C. Irreversible Magnetization Switching Using Surface Acoustic Waves. *Phys. Rev. B* **2013**, *87*, No. 144402.
(37) Chudnovsky, E. M.; Jaafar, R. Manipulating the Magnetization of a Nanomagnet with Surface Acoustic Waves: Spin-rotation Mechanism. *Phys. Rev. Appl.* **2016**, *5*, No. 031002.
(38) Tejada, J.; Chudnovsky, E. M.; Zarzuela, R.; Statuto, N.; Calvo-de la Rosa, J.; Santos, P. V.; Hernández-Mínguez, A. Switching of Magnetic Moment of Nanoparticles by Surface Acoustic Waves. *Europhys. Lett.* **2017**, *118*, No. 37005.
(39) Choi, K. H.; Oh, J. H.; Kim, H. J.; Kim, J. Y.; Lee, S. G.; Rhim, S. M. In *Surface Acoustic Wave Propagation Properties of the Relaxor Ferroelectric PMN−PT Single Crystal*, 2001 IEEE Ultrasonics Symposium, 2001; p 161.
(40) Vansteenkiste, A.; Leliaert, J.; Dvorkik, M.; Helsen, M.; Garcia-Sanchez, F.; van Waeyenberge, B. The Design and Verification of MuMax3. *AIP Adv.* **2014**, *4*, No. 107133.
(41) James, A. M.; Lord, M. P. *Macmillan's Chemical and Physical Data*; Macmillan: London, U.K., 1992.
(42) Park, S.-E.; Shrout, T. R. Ultrahigh Strain and Piezoelectric Behavior in Relaxor Based Ferroelectric Single Crystals. *J. Appl. Phys.* **1997**, *82*, 1804−1811.
(43) Zhang, R.; Jiang, B.; Cao, W. Elastic, Piezoelectric and Dielectric Properties of Multidomain $0.67Pb(Mg_{1/3}Nb_{2/3})O_3$-$0.33PbTiO_3$ Single Crystals. *J. Appl. Phys.* **2001**, *90*, 3471−3475.
(44) Kittel, C. On the Theory of Ferromagnetic Resonance Absorption. *Phys. Rev.* **1948**, *73*, 155−161.
(45) Kumar, D.; Dmytriiev, O.; Ponraj, S.; Barman, A. Numerical Calculation of Spin Wave Dispersions in Magnetic Nanostructures. *J. Phys. D: Appl. Phys.* **2012**, *45*, No. 015001.
(46) Barman, A.; Kruglyak, V. V.; Hicken, R. J.; Rowe, J. M.; Kundrotaite, A.; Scott, J.; Rahman, M. Imaging the Dephasing of Spin Wave Modes in a Square Thin Film Magnetic Element. *Phys. Rev. B* **2004**, *69*, No. 174426.
(47) Salehi-Fashami, M.; Roy, K.; Atulasimha, J.; Bandyopadhyay, S. Magnetization Dynamics, Bennett Clocking and Associated Energy Dissipation in Multiferroic Logic. *Nanotechnology* **2011**, *22*, No. 155201.
(48) Khitun, A.; Nikonov, D. E.; Wang, K. L. Magnetoelectric Spin Wave Amplifier for Spin Wave Logic Circuits. *J. Appl. Phys.* **2009**, *106*, No. 123909.
(49) Cherepov, S.; Amiri, P. K.; Alzate, J. G.; Wong, K.; Lewis, M.; Upadhyaya, P.; Nath, J.; Bao, M.; Bur, A.; Wu, T.; Carman, G. P.; Khitun, A.; Wang, K. L. Electric-field-induced Spin Wave Generation Using Multiferroic Magnetoelectric Cells. *Appl. Phys. Lett.* **2014**, *104*, No. 082403.
(50) Chen, T.; Dumas, R. K.; Eklund, A.; Muduli, P. K.; Houshang, A.; Awad, A. A.; Dürrenfeld, P.; Gunnar Malm, B.; Rusu, A.; Akerman, J. Spin-Torque and Spin-Hall Nano-Oscillators. *Proc. IEEE* **2016**, *104*, 1919−1945.
(51) Yogendra, K.; Fan, D.; Roy, K. Coupled Spin Torque Nano Oscillators for Low Power Neural Computation. *IEEE Trans. Magn.* **2015**, *51*, No. 4003939.
(52) Park, M. G. A.; Baek, S.-H. C.; Park, B. G.; Lee, S.-H. Frequency Control of a Spin-torque Oscillator Using Magnetostrictive Anisotropy. *Appl. Phys. Lett.* **2016**, *108*, No. 023504.
(53) Duan, C. G.; Jaswal, S. S.; Tsymbal, E. Y. Predicted Magnetoelectric Effect in $Fe/BaTiO_3$ Multilayers: Ferroelectric Control of Magnetism. *Phys. Rev. Lett.* **2006**, *97*, No. 047201.

DOI: 10.1021/acsami.8b19243
ACS Appl. Mater. Interfaces 2018, 10, 43970−43977